Suppressing Nonradiative Energy Loss in Ternary Organic Solar Cells Through Elaborate Disruption of Planarity of Guest Acceptor

Qi Liang[a], Xiaodong Wang [a], Hongxiang Li [c], Huanxiang Jiang[a,], Hao Lu [b,]*, Yahui Liu [a,]*, Andong Zhang [a], and Zhishan Bo [a,]**

[a]College of Textiles and Clothing, Qingdao University, Qingdao 266071, P. R. China. E-mail：jianghx@qdu.edu.cn; liuyh@qdu.edu.cn; zsbo@bnu.edu.cn

[b]College of Materials Science and Engineering, Qingdao University, Qingdao, 266071, P. R. China. E-mail：luhao@qdu.edu.cn

[c]College of Polymer Science and Engineering State Key Laboratory of Polymer Materials Engineering Sichuan University Chengdu 610065, China.

1. Experimental section

Photovoltaic solution preparation

The solution of D18:eC9-4F (1:1.2), D18:eC9-4F:Y-PH-X (1:1.2:0.1), D18:eC9-4F:Y-PH-X (1:1.2:0.1) in chloroform was stirred at 90˚C for 30 min, followed by 50˚C for 60 min in a N2-filled glovebox. The concentration of D18 was 4.5mg/mL respectively. D18, eC9-4F, L8-BO, and Y-PH-X were all synthesized with in the laboratory environment.

The PEDOT:PSS solution (Heraeus, AI 4083) was fabricated onto the precleaned ITO substrates followed by annealing at 100 ℃ of 40 min. The solution of photovoltaic materials was spin-coated onto the PEDOT:PSS films in N_2-filled glove box annealing(at 100℃of 1min). Then PDINN (Derthon)/methanol (1mg/mL) was spin-coated accordingly. Finally, 100 nm Ag was thermally evaporated through a shadow mark at a vacuum pressure below 3×10-6 Torr. The effective area for each cell was 0.04 cm^2.

Characterizations of films

UV-visible absorption spectra were measured at ambient conditions on a PerkinElmer UV-vis spectrometer model Lambda 750. Surface morphology information of the active layer was obtained by using Atomic force microscopy (AFM

Digital Instrument Multimode Nanoscope IIIA in tap mode).

Energy loss (E_{loss}) calculations

The ΔE_{nr} values of devices were evaluated by the electroluminescence external quantum efficiency (EQE_{EL}) according to the equation: $\Delta E_{nr} = -kT\ln(EQE_{EL})$, where k and T represent the Boltzmann constant and temperature in Kelvin, respectively. [1]

Charge mobility measurement by SCLC method

The architectures of ITO/ZnO/Active layer/PDINN/Ag and ITO/PEDOT:PSS/Active layer/MoO3/Ag were used for electron and hole mobility measurement, respectively. The mobilities were calculated according to the Mott-Gurney equation: $J = 9\varepsilon\varepsilon_0\mu/(8L^3)V^2$,where J is the current density; ε is the dielectric constant of the blend film; ε_0 is the permittivity of the vacuum; μ is the mobility; L is the thickness of the film; $V = V_{appl}$-V_{bi}, V_{appl} and V_{bi} are the applied voltage to the device and the build-in voltage, respectively.[2]

J-V and EQE Measurement

The J-V curves of the devices were measured in a glove box with an instrument from Enli Technology Ltd., Taiwan (SS-F53A) under AM 1.5G illumination (AAA class solar simulator, 100 mW cm^{-2} calibrated with a standard single crystal Si photovoltaic cell). EQE measurements were performed by a solar cell spectral response measurement system (QER3011, Enli Technology Co. Ltd), and the intensity was calibrated with a standard single-crystal Si photovoltaic cell before the test.

PLQY and FL intensity

The steady-state photoluminescent spectra and photoluminescence quantum yield (PLQY) values were all recorded on the HORIBA Nanolog.

GIWAXS and GISAXS Measurement

The GIWAXS data were obtained at 1W1A Diffuse X-ray Scattering Station, Beijing Synchrotron Radiation Facility (BSRF-1W1A).GISAXS data of films were obtained at beamline BL16B1 of Shanghai Synchrotron Radiation Facility (SSRF).[3] The incidence angle was 0.2°, and the sample-to-detector distance was 2200 mm by calibration for GISAXS. The GISAXS 1D profiles were fitted with a universal

modelfollowingEquation. Data fitting was done using SasView (version 5.01) software.

$$I(q) = 1 + \frac{A_1}{[1 + (q\xi)^2]^2} + A_2\langle P(q,R)\rangle S(q,R,\eta,D) + B$$

$$S(q) = 1 + \frac{sin[(D-1)tan^{-1}(q\eta)]b \pm \sqrt{b^2-4ac}}{(qR)^D} \quad \frac{D\Gamma(D-1)}{[1 + 1/(q\eta)^2]^{(D-1)/2}}$$

where A1, A2, and B are independent fitting parameters and q is the scattering wave vector. The average correlation length ξ of the D18 domain and the Debye-Andersone-Brumberger (DAB) term make up the first term. The contribution from eC9-4F fractal-like aggregations is seen in the second term. Here, R is the mean spherical radius of the primary BTP-eC9-4F particles, P (q, R) is the form factor of the eC9-4F, S (q, R, η, D) is the fractal structure factor to explain the primary particles interaction in this fractal-like aggregation system, η is the correlation length of the fractal-like structure of eC9-4F, and D is the fractal dimension of the network of eC9-4F. Equation 3 was used to calculate the average domain size by the Guinier radius of the fractal-like network Rg of eC9-4F.

$$R_g = \eta\sqrt{D(D+1)/2}$$

Materials and Synthesis.

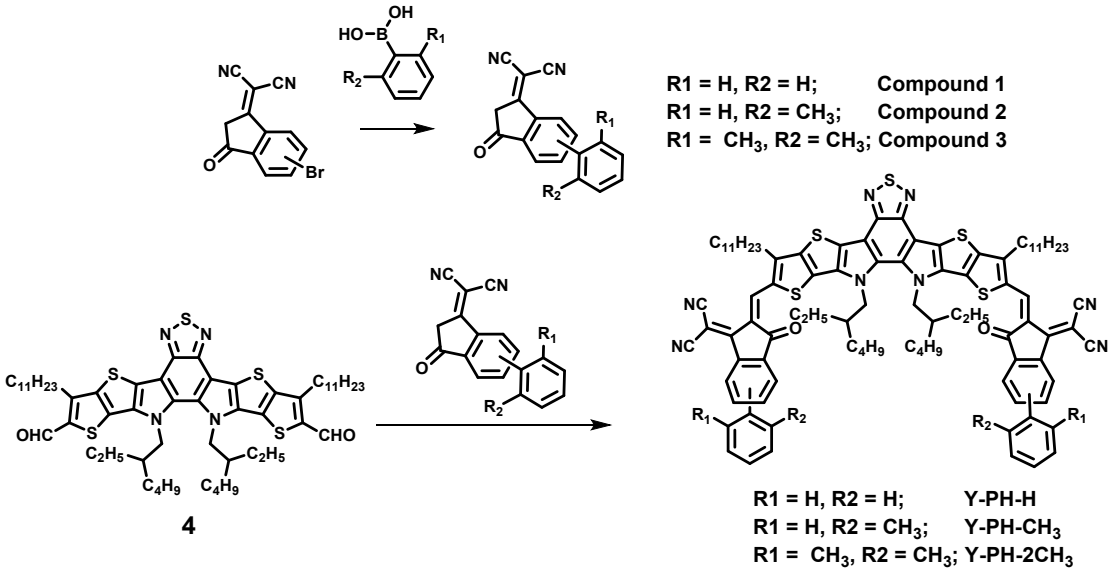

Synthesis of compound **1**

2-(5 or 6 -bromo-3-oxo-2,3-dihydro-1H-inden-1-ylidene)malononitrile (300 mg;

1.10 mmol), phenylboronic acid (201 mg;1.65 mmol) and K_2CO_3 (1.52 g; 11 mmol)were dissolved into tetrahydrofuran (30 ml) and water (10 ml)in a three-neck flask. After the solution was flushed with nitrogen for 15min, $Pd(PPh_3)_4$ (30 mg) was added to the solution, then let the solution temperature to 80°C for 20 h. Washed with saturated salt water and ethyl acetate, the ethyl acetate was removed under reduced pressure. The crude product was subsequently purified by column chromatography on silica gel to afford compound **1** (277 mg, 93% yield). ^{1}H NMR (400 MHz, $CDCl_3$) δ: 8.82 (s, 0.62H), 8.68-8.69 (d, *J* = 4 Hz, 0.38H), 8.16 (s, 0.34H), 8.09-8.11 (d, *J* = 8 Hz, 0.35H), 8.05-8.07 (d, *J* = 8 Hz, 0.65H), 8.01-8.03 (d, *J* = 8 Hz, 0.65H), 7.66-7.68 (m, 2H), 7.47-7.54 (m, 3H), 3.75 (s, 2H). ^{13}C NMR (400 MHz, $CDCl_3$) δ: 195.04, 194.45, 166.51, 165.86, 149.50, 148.89, 143.24,141.37, 141.14, 139.10, 138.27, 137.98, 134.74, 129.66, 129.59, 129.54, 127.61, 127.51, 126.60, 125.17, 124.05, 122.52, 120.78, 115.37, 112.46, 112.34, 112.14, 43.69.

Synthesis of compound **2**

2-(5 or 6 -bromo-3-oxo-2,3-dihydro-1H-inden-1-ylidene)malononitrile (300 mg; 1.10 mmol), o-tolylboronic acid (224 mg;1.65 mmol) and K_2CO_3 (1.52 g; 11 mmol)were dissolved into tetrahydrofuran (30 ml) and water (10 ml)in a three-neck flask. After the solution was flushed with nitrogen for 15min, $Pd(PPh_3)_4$ (30 mg) was added to the solution, then let the solution temperature to 80°C for 20 h. Washed with saturated salt water and ethyl acetate, the ethyl acetate was removed under reduced pressure. The crude product was subsequently purified by column chromatography on silica gel to afford compound **2** (285 mg, 91% yield). ^{1}H NMR (400 MHz, $CDCl_3$) δ: 8.67-8.68 (d, *J* = 4 Hz, 0.41H), 8.59 (s, 0.56H), 8.01-8.02 (d, *J* = 4 Hz, 0.56H), 7.93 (s, 0.40H), 7.85-7.86 (d, *J* = 4 Hz, 0.40H), 7.80-7.81 (d, *J* = 4 Hz, 0.58H), 7.29-7.37 (m, 3H), 7.22-7.24 (m, 1H), 3.76 (s, 2H), 2.99-2.31 (m, 3H). ^{13}C NMR (400 MHz, $CDCl_3$) δ: 194.94, 194.52, 166.48, 166.08, 150.61, 150.32, 142.58,140.98, 140.73, 139.00, 138.92, 137.28, 137.06, 135.18, 131.16, 131.11, 129.61, 129.10, 126.55, 126.52, 126.38, 125.90, 125.09, 124.58, 112.41, 112.27, 112.22, 112.16, 43.65, 43.62, 20.59, 20.46.

Synthesis of compound **3**

2-(5 or 6 -bromo-3-oxo-2,3-dihydro-1H-inden-1-ylidene) malononitrile (300 mg; 1.10 mmol), (2,6-dimethylphenyl) boronic acid (247 mg;1.65 mmol) and K_2CO_3 (1.52 g; 11 mmol) were dissolved into tetrahydrofuran (30 ml) and water (10 ml)in a three-neck flask. After the solution was flushed with nitrogen for 15min, $Pd(PPh_3)_4$ (30 mg) was added to the solution, then let the solution temperature to 80°C for 20 h. Washed with saturated salt water and ethyl acetate, the ethyl acetate was removed under reduced pressure. The crude product was subsequently purified by column chromatography on silica gel to afford compound **3** (289 mg, 88% yield). ^{1}H NMR (400 MHz, $CDCl_3$) δ: 8.70-8.72 (d, *J* = 8 Hz, 0.44H), 8.41 (s, 0.54H), 8.04-8.05 (d, *J* = 4 Hz, 0.54H), 7.79 (s, 0.45H), 7.69-7.71 (d, *J* = 8 Hz, 0.46H), 7.64-7.66 (d, *J* = 4 Hz, 0.56H), 7.22-7.25 (m, 1H), 7.14-7.15 (m, 2H), 3.77 (s, 2H), 2.04 (s, 3H) , 2.01 (s, 3H). ^{13}C NMR (400 MHz, $CDCl_3$) δ: 194.91, 194.53, 166.44, 166.18, 150.34, 150.09, 142.99, 141.16, 139.21, 138.93, 137.56, 137.37, 135.26, 129.10, 128.58, 128.07, 127.98, 126.61, 126.31, 125.44, 124.91, 112.39, 112.26, 112.17, 43.63, 43.58, 20.98, 20.88.

Synthesis of compound **Y-PH-H**

A mixture of compound **4** (150 mg, 0.15 mmol) and compound **1** (120 mg, 0.45 mmol) in chloroform (20 mL) was carefully degassed and pyridine (0.5 mL) was added. The mixture was stirred and refluxed under nitrogen overnight, and the solvent was removed under reduced pressure. The crude product was purified on silica gel chromatography using dichloromethane/petroleum ether (2:1, v/v) as an eluent to obtain the target compound **Y-PH-H** (204 mg, 89%). ^{1}H NMR (400 MHz, $CDCl_3$) δ: 9.15 (s, 2H), 8.92 (s, 1.34H), 8.73-8.74 (d, *J* = 4 Hz, 0.65H), 8.18 (s, 0.67H), 8.01-8.03 (d, *J* = 8 Hz, 1.36H), 7.97-7.99 (m, 2H), 7.68-7.73 (m, 4H), 7.45-7.54 (m, 6H), 4.77-4.78 (m, 4H), 3.23 (m, 4H), 2.13-2.17 (m, 2H), 1.86-1.89 (m, 4H), 1.50-1.52 (m, 4H), 1.36-1.38 (m, 4H), 1.20-1.23 (m, 34H), 0.86-0.88 (m, 6H), 0.77-0.79 (m, 6H), 0.64-0.69 (m, 6H).

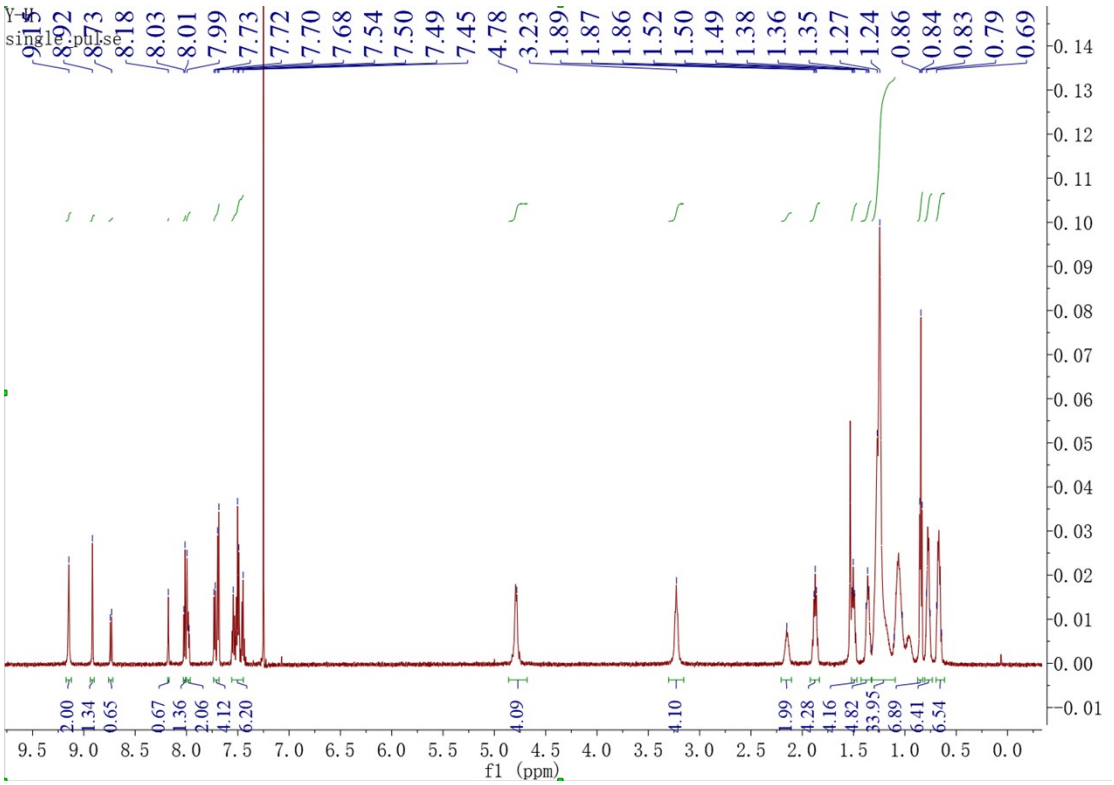

Fig S1 ^{1}H NMR spectrum of **Y-PH-H** in $CDCl_3$.

Synthesis of compound **Y-PH-CH$_3$**

A mixture of compound **4** (150 mg, 0.15 mmol) and compound **2** (128 mg, 0.45 mmol) in chloroform (20 mL) was carefully degassed and pyridine (0.5 mL) was added. The mixture was stirred and refluxed under nitrogen overnight, and the solvent was removed under reduced pressure. The crude product was purified on silica gel chromatography using dichloromethane/petroleum ether (2:1, v/v) as an eluent to obtain the target compound **Y-PH-CH$_3$** (201 mg, 86%). ^{1}H NMR (400 MHz, $CDCl_3$) δ: 9.18 (s, 2H), 8.74-8.75 (m, 0.71H), 8.68 (s, 1.24H), 7.99-8.01 (m, 1.21H), 7.92-7.93 (m, 0.73H), 7.72-7.74 (m, 2H), 7.29-7.36 (m, 8H), 4.75-4.79 (m, 4H), 3.23-3.26 (m, 4H), 2.34-2.36 (m, 6H), 2.09-2.14 (m, 2H), 1.87-1.90 (m, 4H), 1.50-1.53 (m, 4H), 1.36-1.38 (m, 4H), 1.25-1.29 (m, 34H), 0.84-0.86 (m, 6H), 0.74-0.76 (m, 6H), 0.63-0.66 (m, 6H).

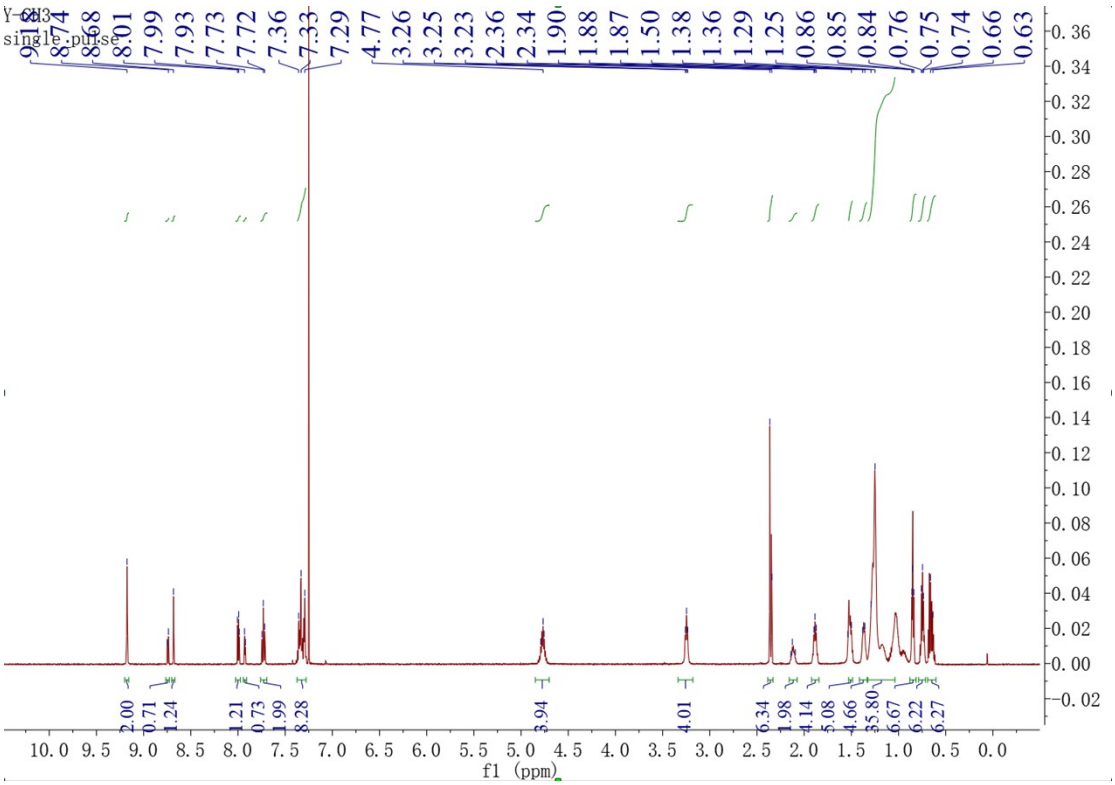

Fig S2 ^{1}H NMR spectrum of **Y-PH-CH$_3$** in $CDCl_3$.

Synthesis of compound **Y-PH-2CH$_3$**

A mixture of compound **4** (150 mg, 0.15 mmol) and compound **3** (134 mg, 0.45 mmol) in chloroform (20 mL) was carefully degassed and pyridine (0.5 mL) was added. The mixture was stirred and refluxed under nitrogen overnight, and the solvent was removed under reduced pressure. The crude product was purified on silica gel chromatography using dichloromethane/petroleum ether (2:1, v/v) as an eluent to obtain the target compound **Y-PH-CH$_3$** (210 mg, 88%). ^{1}H NMR (400 MHz, $CDCl_3$) δ: 9.19-9.21 (m, 2H), 8.77-8.79 (m, 0.83H), 8.49-8.50 (m, 1.14H), 8.00-8.02 (m, 1.13H), 7.75-7.76 (m, 0.86H), 7.54-7.58 (m, 2H), 7.21-7.25 (m, 2H), 7.14-7.18 (m, 4H), 4.74-4.79 (m, 4H), 3.24-3.27 (m, 4H), 2.06-2.07 (m, 14H), 1.87-1.92 (m, 4H), 1.51-1.53 (m, 4H), 1.35-1.39 (m, 4H), 1.36-1.38 (m, 4H), 1.13-1.30 (m, 34H), 0.84-0.87 (m, 6H), 0.71-0.74 (m, 6H), 0.60-0.67 (m, 6H).

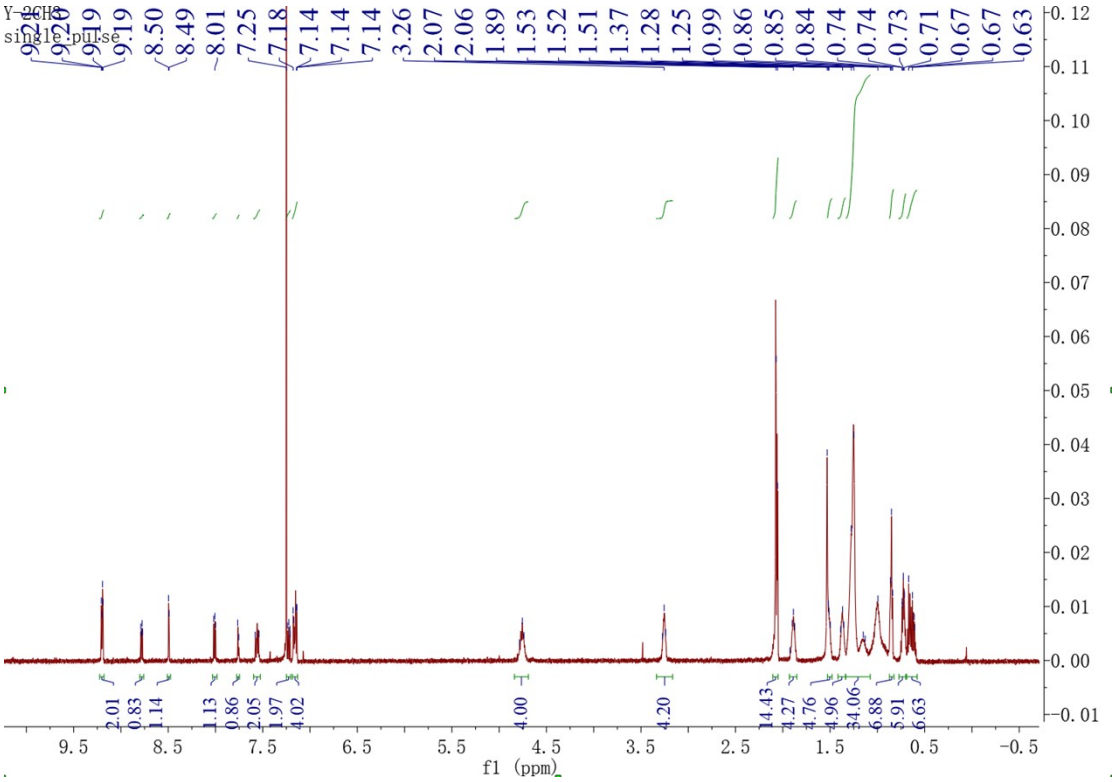

Fig S3 ^{1}H NMR spectrum of **Y-PH-2CH$_3$** in $CDCl_3$.

2. Supporting Figures

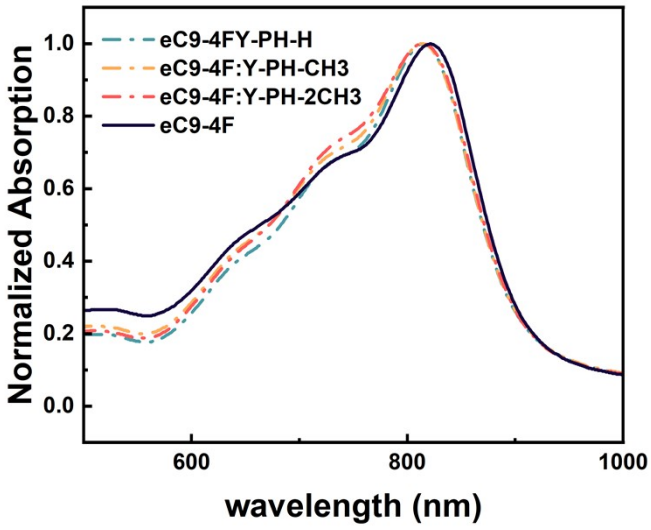

Figure S4. Normalized absorption spectra of eC9-4F, eC9-4F:Y-PH-H, eC9-4F:Y-PH-CH_3, eC9-4F:Y-PH-2CH_3 films.

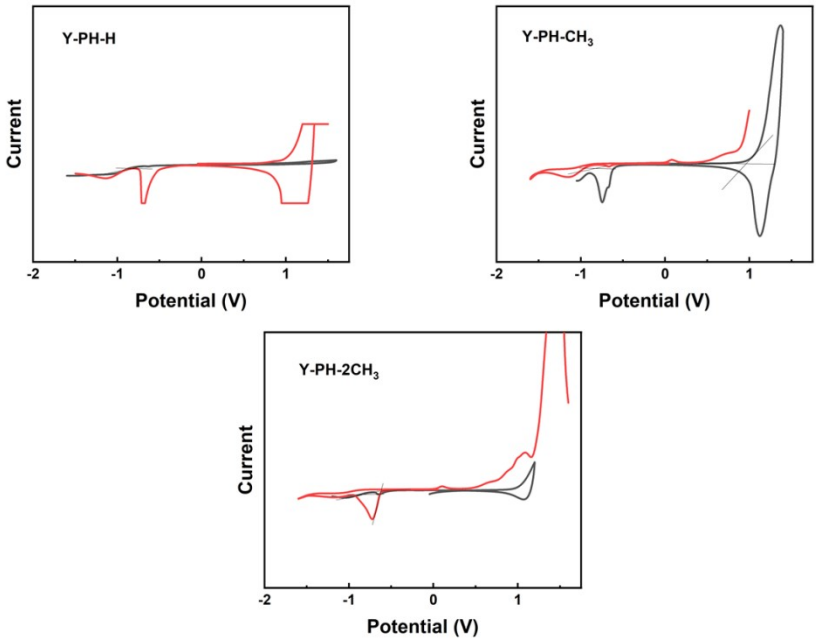

Figure S5. Cyclic voltammogram (CV) curves of Y-PH-H; Y-PH-CH_3 and Y-PH-$2CH_3$.

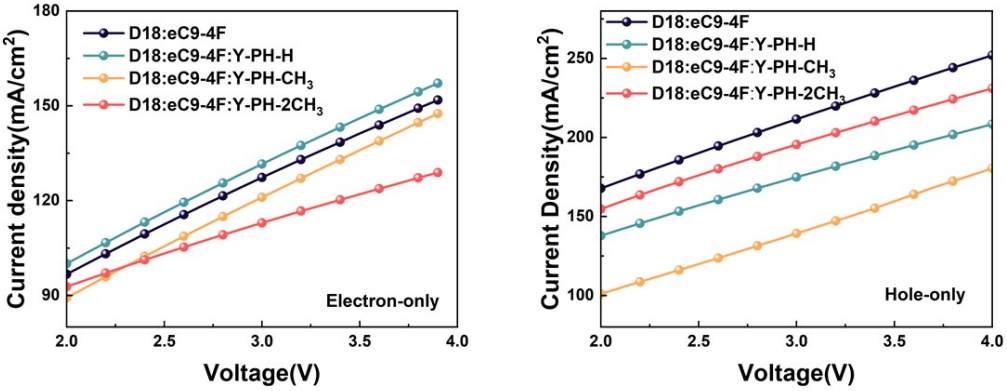

Figure S6. J-V curves of (a) electron-only and (b) hole-only diodes based on D18:eC9-4F,D18:eC9-4F:Y-PH-H,D18:eC9-4F:Y-PH-CH3,D18:eC9-4F:Y-PH-2CH3.

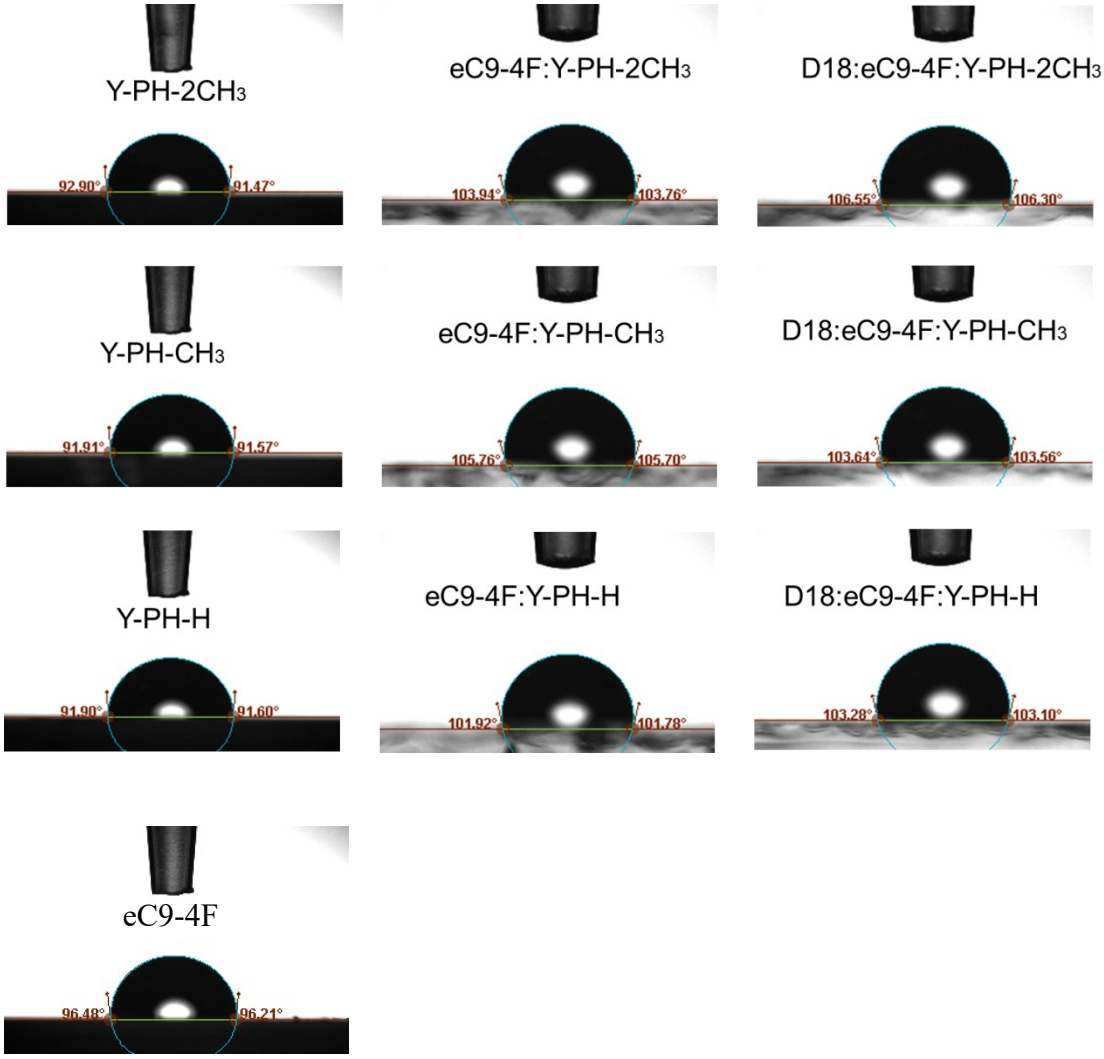

Figure S7. Contact angles of pure and blend films of Y-PH-H, Y-PH-CH3, Y-PH-2CH3, Ec9-4F, and D18.

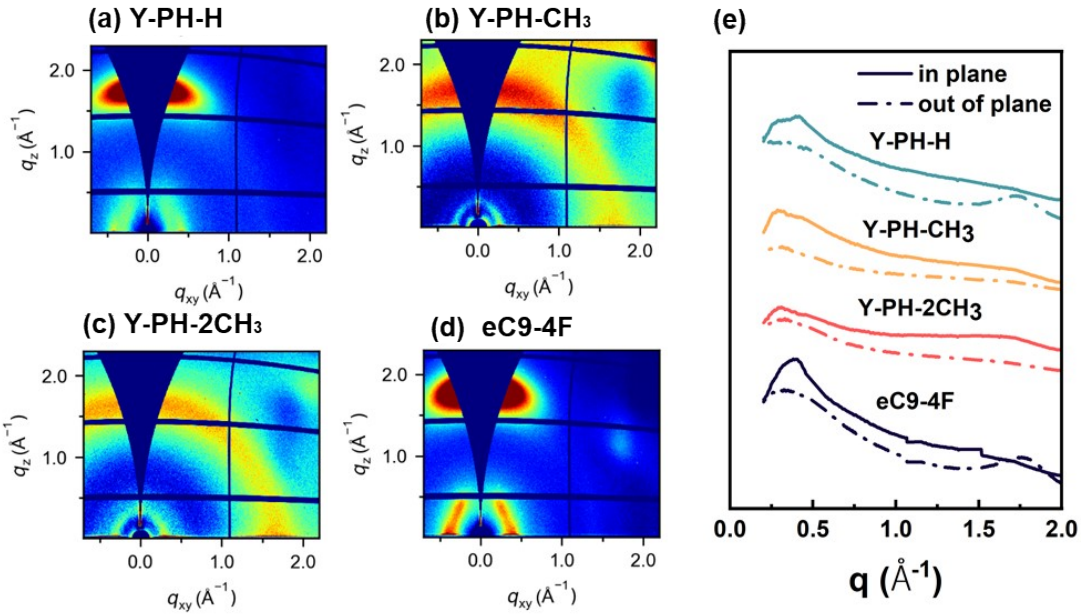

Figure S8. GIWAXS patterns of eC9-4F, Y-PH-H, Y-PH-CH3, Y-PH-2CH3 films, and the line profiles of GIWAXS in plane.

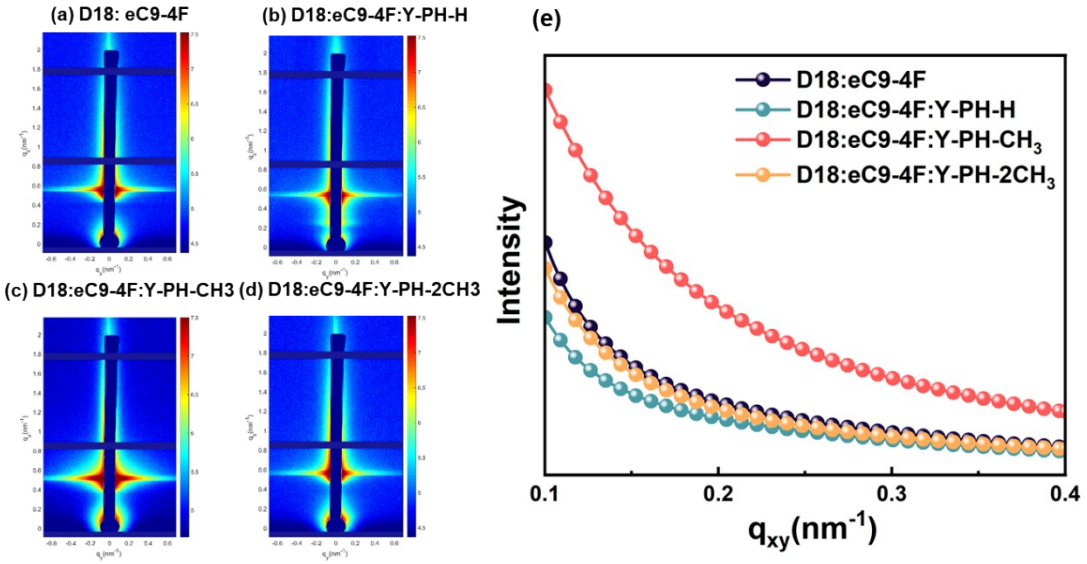

Figure S9. GISAXS patterns of D18:eC9-4F, D18: eC9-4F:Y-PH-H, D18:eC9-4F:Y-PH-CH3, D18:eC9-4F:Y-PH-2CH3, and the line profiles of GISAXS results.

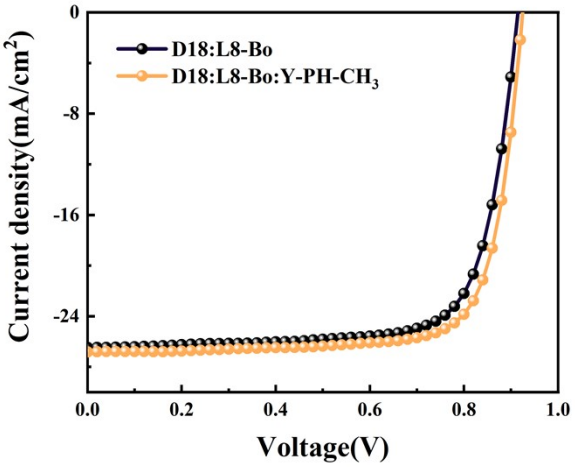

Figure S10. J-V curves of the D18:L8-BO binary and D18:L8-BO:-PH-CH_3 ternary devices.

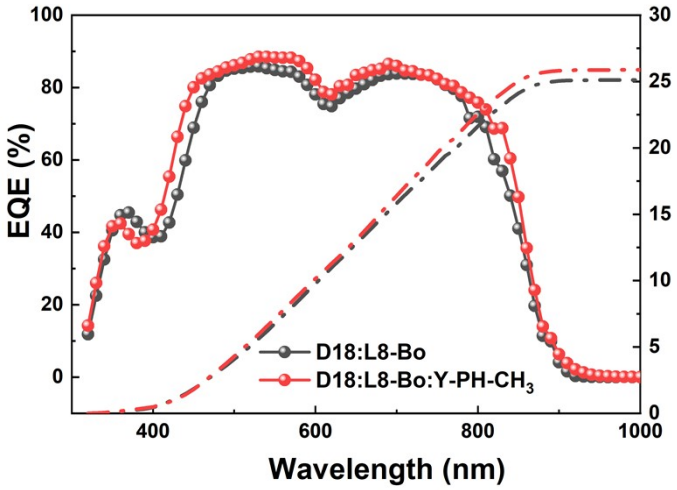

Figure S11. EQE curves of the D18:L8-BO binary and D18:L8-BO:Y-PH-CH_3 ternary devices.

Figure S12. The PLQY of eC9-4F, eC9-4F:Y-PH-H, eC9-4F:Y-PH-CH3, eC9-4F:Y-PH-2CH3.

Figure S13 [4-19]

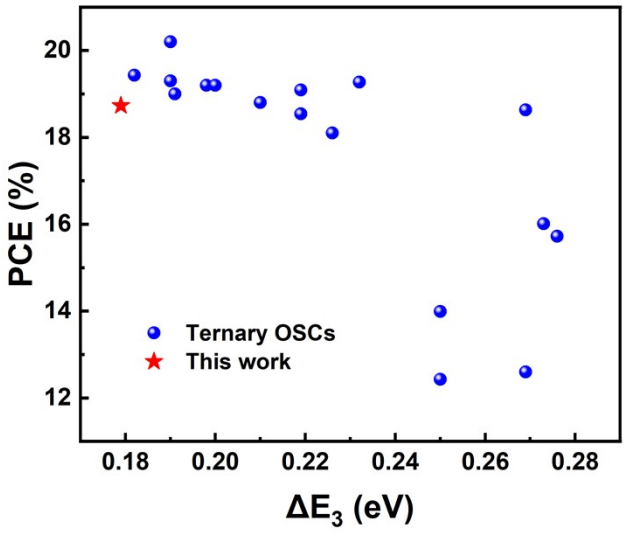

3. Supporting Tables

Table S1. The charge mobilities of D18:eC9-4F, D18: eC9-4F:Y-PH-H, D18: eC9-4F:Y-PH-CH3, D18:eC9-4F:Y-PH-2CH3 films.

	μ_e×10^{-4} ($cm^2V^{-1}s^{-1}$)	μ_h×10-4 ($cm^2V^{-1}s^{-1}$)	μ_e/μ_h
D18:eC9-4F	3.76	3.19	1.18
D18:eC9-4F:Y-PH-H	6.65	6.14	1.08
D18:eC9-4F:Y-PH-CH3	7.13	6.88	1.03
D18:eC9-4F:Y-PH-2CH3	8.39	5.85	1.43

Table S2. The PLQY of D18:eC9-4F, D18: eC9-4F:Y-PH-H, D18: eC9-4F:Y-PH-CH3, D18:eC9-4F:Y-PH-2CH3 films.

	PLQY(Pure film)	PLQY(Bend film)
D18:eC9-4F	4.19	
D18:eC9-4F:Y-PH-H	4.80	4.87
D18:eC9-4F:Y-PH-CH3	5.29	5.95
D18:eC9-4F:Y-PH-2CH3	5.88	7.45

Table S3. A summary of *d*-spacing and coherence lengths (CCL) of D18:eC9-4F, D18: eC9-4F:Y-PH-H, D18: eC9-4F:Y-PH-CH3, D18:eC9-4F:Y-PH-2CH3 films.

	FWHM（nm）	CCL（nm）	q（Å）	$d_{\pi\text{-}\pi}$(nm）
D18:eC9-4F	0.251	22.558	1.725	3.642
D18:eC9-4F:Y-PH-H	0.242	23.333	1.7425	3.606
D18:eC9-4F:Y-PH-CH3	0.237	23.865	1.7425	3.606
D18:eC9-4F:Y-PH-2CH3	0.284	19.923	1.725	3.642

Table S4. Fitting parameters of D18:eC9-4F, D18: eC9-4F:Y-PH-H, D18: eC9-4F:Y-PH-CH3, D18:eC9-4F:Y-PH-2CH3 films, where ξ, 2*R*g, and *D* are obtained from GISAXS fitting.

	ξ (nm)	η(nm)	D	2Rg(nm)
D18:eC9-4F	25.7	7.1	2.5	29.7
D18:eC9-4F:Y-PH-H	26.3	7.2	2.5	30.1
D18:eC9-4F:Y-PH-CH3	27.8	7.8	2.7	34.9
D18:eC9-4F:Y-PH-2CH3	19.8	6.4	2.1	23.1

Table S5. Device performance parameters of ternary OSCs at different weight ratios.

1:1.2:0.1	Voc(V)	FF(%)	Jsc(mA/cm2)	PCE(%)
D18:eC9-4F	0.869	71.23	27.76	17.21
D18:eC9-4F:Y-PH-H	0.874	72.77	27.89	17.75
D18:eC9-4F:Y-PH-CH_3	0.881	75.58	27.95	18.63
D18:eC9-4F:Y-PH-$2CH_3$	0.887	69.59	26.52	16.39
1:1.2:0.05				
D18:eC9-4F:Y-PH-H	0.866	68.93	25.16	15.03
D18:eC9-4F:Y-PH-CH_3	0.869	70.35	24.86	15.21
D18:eC9-4F:Y-PH-$2CH_3$	0.873	67.92	24.43	14.49
1:1.2:0.15				
D18:eC9-4F:Y-PH-H	0.879	69.44	24.67	14.95
D18:eC9-4F:Y-PH-CH_3	0.899	71.11	23.99	15.31
D18:eC9-4F:Y-PH-$2CH_3$	0.907	66.29	22.94	13.76

[1] J. Benduhn, K. Tvingstedt, F. Piersimoni, S. Ullbrich, Y. Fan, M. Tropiano, K. A. McGarry, O. Zeika, M. K. Riede, C. J. Douglas, Intrinsic non-radiative voltage losses in fullerene-based organic solar cells, Nature Energy 2 (2017) 1-6.

[2] B. Zhang, N. An, H. Wu, Y. Geng, Y. Sun, Z. Ma, W. Li, Q. Guo, E. Zhou, The first application of isoindigo-based polymers in non-fullerene organic solar cells, Sci. China Chem. 63 (2020) 1262-1271.

[3] Z. Peng, K. Xian, J. Liu, Y. Zhang, X. Sun, W. Zhao, Y. Deng, X. Li, C. Yang, F. Bian, Unraveling the Stretch-Induced Microstructural Evolution and Morphology–Stretchability Relationships of High-Performance Ternary Organic Photovoltaic Blends, Adv. Mater. 35 (2023) 2207884.

[4] X. Cui, G. Ran, H. Lu, Y. Liu, H. Jiang, H. Zhang, D. Li, Y. Liu, Y. Lin, Z. Ma, W. Zhang, P. Cheng, Z. Bo, Enabling Low Nonradiative Recombination Losses in Organic Solar Cells by Efficient Exciton Dissociation, Adv. Funct. Mater. 34 (2024) 2400219.

[5] X. Jiang, X. Wang, Y. Wang, G. Ran, W. Liu, H. Lu, H. Li, N. Wei, Z. Wei, Y. Lin, Z. Ma, Y. Liu, W. Zhang, X. Xu, Z. Bo, Achieving 19.78%-Efficiency Organic Solar Cells by 2D/1A Ternary Blend Strategy with Reduced Non-Radiative Energy Loss, Adv. Funct. Mater. 34 (2024) 2406744.

[6] Y. Jiang, S. Sun, R. Xu, F. Liu, X. Miao, G. Ran, K. Liu, Y. Yi, W. Zhang, X. Zhu, Non-fullerene acceptor with asymmetric structure and phenyl-substituted alkyl side chain for 20.2%

efficiency organic solar cells, Nat. Energy 9 (2024) 975-986.

[7] S. Lai, Y. Cui, Z. Chen, X. Xia, P. Zhu, S. Shan, L. Hu, X. Lu, H. Zhu, X. Liao, Y. Chen, Impact of Electrostatic Interaction on Vertical Morphology and Energy Loss in Efficient Pseudo-Planar Heterojunction Organic Solar Cells, Adv. Mater. 36 (2024) 2313105.

[8] W. Liang, L. Chen, Z. Wang, Z. Peng, L. Zhu, C. H. Kwok, H. Yu, W. Xiong, T. Li, Z. Zhang, Y. Wang, Y. Liao, G. Zhang, H. Hu, Y. Chen, Oligothiophene Additive-Assisted Morphology Control and Recombination Suppression Enable High-Performance Organic Solar Cells, Adv. Energy Mater. 14 (2024) 2303661.

[9] H. Liu, T. Shan, N. Yu, N. Zheng, L. Zhu, Z. Ma, M. Zhu, Suppress energy loss to boost power conversion efficiency of organic photovoltaics with linear side chains modulation, Org. Electron. 128 (2024) 107019.

[10] Z. Liu, C. Zhu, J. Xu, Y. Xu, J. Zeng, J. Wang, J. Zhang, P. Zhu, D. Wang, X. Zhou, Y. Zhang, X. Wang, L. Ying, L. Yan, B. Xu, Enhancing organic solar cell efficiency with ester-based quinoxaline non-fullerene acceptors in ternary blends, Nano Energy 137 (2025) 110801.

[11] H. Lu, D. Li, W. Liu, G. Ran, H. Wu, N. Wei, Z. Tang, Y. Liu,

W. Zhang, Z. Bo, Designing A–D–A Type Fused-Ring Electron Acceptors with a Bulky 3D Substituent at the Central Donor Core to Minimize Non-Radiative Losses and Enhance Organic Solar Cell Efficiency, Angew. Chem. Int. Ed. 63 (2024) e202407007.

[12] D. Luo, L. Zhang, L. Li, T. Dai, E. Zhou, M. Quan, H. Zhang, A. K. K. Kyaw, W.-Y. Wong, Small Singlet–Triplet Gap Terpolymer Donor with a Simple Pt Complex Enables Organic Solar Cells with Low Energy Loss and Over 19.2% Efficiency, Adv. Sci. n/a 2410154.

[13] J. Ren, S. Zhang, Z. Chen, T. Zhang, J. Qiao, J. Wang, L. Ma, Y. Xiao, Z. Li, J. Wang, X. Hao, J. Hou, Optimizing Molecular Packing via Steric Hindrance for Reducing Non-Radiative Recombination in Organic Solar Cells, Angew. Chem. Int. Ed. 63 (2024) e202406153.

[14] X. Si, Y. Huang, W. Shi, R. Wang, K. Ma, Y. Zhang, S. Wu, Z. Yao, C. Li, X. Wan, Y. Chen, Achieving Organic Solar Cells with an Efficiency of 18.80% by Reducing Nonradiative Energy Loss and Tuning Active Layer Morphology, Adv. Funct. Mater. 33 (2023) 2306471.

[15] Z. Sun, H. Ma, S. Yang, Y. Cho, S. Lee, J. Park, T. L. H. Mai, W. Kim, S. Jeong, S. Kim, C. Yang, Insight Into Designing

High-Performance Polythiophenes for Reduced Urbach Energy and Nonradiative Recombination in Organic Solar Cells, Adv. Funct. Mater. 34 (2024) 2403093.

[16] H. Wu, H. Lu, Y. Li, X. Zhou, G. Zhou, H. Pan, H. Wu, X. Feng, F. Liu, K. Vandewal, W. Tress, Z. Ma, Z. Bo, Z. Tang, Decreasing exciton dissociation rates for reduced voltage losses in organic solar cells, Nat. Commun. 15 (2024) 2693.

[17] R. Xu, Y. Jiang, F. Liu, G. Ran, K. Liu, W. Zhang, X. Zhu, High Open-Circuit Voltage Organic Solar Cells with 19.2% Efficiency Enabled by Synergistic Side-Chain Engineering, Adv. Mater. 36 (2024) 2312101.

[18] Z. Zheng, J. Wang, P. Bi, J. Ren, Y. Wang, Y. Yang, X. Liu, S. Zhang, J. Hou, Tandem Organic Solar Cell with 20.2% Efficiency, Joule 6 (2022) 171-184.

[19] J. Zhu, Z. Qin, A. Lan, S. Jiang, J. Mou, Y. Ren, H. Do, Z.-K. Chen, F. Chen, A-D-A Type Nonfullerene Acceptors Synthesized by Core Segmentation and Isomerization for Realizing Organic Solar Cells with Low Nonradiative Energy Loss, Small 20 (2024) 2305529.